Simulation and Experiment of Distorted LFM Signals in Shallow Water Environment

*Young-Nam Na, *Mun-Sub Jung, *Tae-Bo Shim, and **Chun-Duck Kim

Abstract

This paper attempts to examine the characteristics of underwater acoustic signals distorted in shallow water environments. Time signals are simulated using an acoustic model that employs the Fourier synthesis scheme. An acoustic experiment was conducted in the shallow sea near Pohang, Korea, where water depth is about 60 m. The environment in the simulation is set up so that it approximates the experimental condition, which can be regarded as range-independent. The signal is LFM (linear frequency modulated) type centered on one of the four frequencies 200, 400, 600 and 800 Hz, each being swept up or down with the bandwidth of 100 Hz. To analyze the signal characteristics, the study introduces a spectrum estimation scheme, pseudo Wigner-Ville distribution (PWVD). The simulated and measured signals suffer great interference by the interactions of neighboring rays. Although there are constructive or destructive interference, the signals keep LFM characteristics well. This is thought that only a few dominant rays of small loss contribute to the received signals in a shallow water environment.

I. Introduction

Within the frame of linear acoustics there are fundamentally two approaches to broadband modeling problem: Fourier synthesis and direct computation [1]. The first is to solve the pulse propagation via the frequency domain by Fourier synthesis of CW results. This approach is attractive since it requires little programming effort. That is, any of the time-harmonic acoustic models can be linked up with a pulse post-processor which numerically performs the Fourier synthesis based on a number of CW calculations with the frequency band of interest. The Fourier synthesis scheme is adopted to simulate the LFM signals distorted in the environment. In the CW calculation with each frequency an acoustic model based on the parabolic equation (PE) is applied.

The LFM signals are chosen in this study because they are relatively simple to be generated but enable to analyze the distorted signals with ease. They are regarded to be enough to accommodate the signal distortion caused by the environment.

Few papers have been published to deal with the LFM signals distorted by surrounding environment. Field et al. [2] tried to simulate the signals distorted in the deep water environment using a time-domain PE (TDPE) model. They considered relatively short range (5 km) compared with the water depth (1.3 km). In these conditions the traveling waves suffer one surface or/and bottom interaction, yielding small distortion and loss.

This study assumes the environment to be shallow water, and considers environmental variations in sound speed profile and bottom property. The principal characteristics of shallow water propagation is that the sound speed profile is downward decreasing or nearly constant over depth, meaning that long-range propagation takes place exclusively via bottom-interacting paths [1]. Hence, the important paths are either refracted bottom-reflected or surface-reflected-bottom-reflected. Typical shallow water environments are found on the continental shelf for water depth down to 200 m. The signals inevitably undergo distortions by the environment in which they propagate.

This paper is directed to examining the characteristics of low-frequency LFM signals distorted in shallow water environments. Section II describes the theories employed in this study such as Fourier synthesis and spectrum estimation. Section III delivers the simulation results with LFM signals. The simulation is conducted by varying sound speed profile, bottom property and source-receiver range. Section IV presents the results with the experimental data. Section V gives the conclusions derived in this study.

II. Theory

A. Fourier Synthesis of Frequency-Domain Solution

The inhomogeneous Helmholtz equation for a simple

* Agency for Defense Development, Chinhae
** Pukyong National University, Pusan

Manuscript Received : March 23, 1998.

point source of strength $S(\omega)$ at point r_o is given by

$$[\nabla^2 + k^2] P(\omega, r) = S(\omega)\,\delta(r - r_o), \tag{1}$$

where P is pressure field at frequency ω and position r, and δ is dirac delta function.

The solution of the time-dependent wave equation can be obtained by an inverse Fourier transform of the frequency-domain solution as

$$p(r, z, t) = \frac{1}{2\pi} \int_{-\infty}^{\infty} S(\omega) P(r, z, \omega)\, e^{i\omega t} d\omega, \tag{2}$$

where $S(\omega)$ is the source spectrum and $P(r, z, \omega)$ is the spatial transfer function. Here, it is assumed that the environment could be described in a cylindrical coordinates (i.e., azimuthal variations are negligible). The main computational effort is to find the transfer function at a number of discrete frequencies within the frequency band of interest. The calculation of the integral in Eq. (2) is then done by an fast Fourier transform (FFT) at each spatial position (r, z) for which the pulse response is desired.

Assuming that the source does not produce any significant energy above a certain frequency ω_{max}, Eq. (2) is replaced by

$$p(r, z, t) = \frac{1}{2\pi} \int_{-\omega_{max}}^{\omega_{max}} S(\omega) P(r, z, \omega)\, e^{i\omega t} d\omega, \tag{3}$$

where $P(r, z, \omega)$ represents a normalized transfer function. So, if $P(r, z, \omega)$ represents pressure field (transmission loss pressure), then $S(\omega)$ is the frequency spectrum of the source pressure at 1-m distance from the source. To yield a real time series, it is necessary to include the negative spectrum in the integration, or alternatively to use the form

$$p(r, z, t) = \mathrm{Re}\{\frac{1}{\pi} \int_{0}^{\omega_{max}} S(\omega) P(r, z, \omega)\, e^{i\omega t} d\omega\}. \tag{4}$$

The solution to the Helmholtz equation (1) is conjugate symmetric, i.e., $P(r, z, -\omega) = \overline{P(r, z, \omega)}$, where $\overline{P(\,)}$ means complex conjugate of $P(\,)$. In this paper, a LFM signal is generated and its spectrum is imposed on the Fourier synthesis as the source spectrum $S(\omega)$.

Eq. (4) is a continuous form to evaluate pressure field at each time t. To be practically applicable, the pressure field should be expressed in discrete form from which time signal can be obtained at each time step.

Let us assume that the response at a point (r, z) is sought in a time window of length T, starting at some time t_{min}. The time and frequency axes are then discretized as

$$\begin{aligned} t_i &= t_{min} + i\Delta t, \quad i = 0, 1, 2, \ldots (N-1), \\ \omega_l &= l\Delta\omega, \qquad l = -(N/2-1), \ldots (N/2-1), \end{aligned} \tag{5}$$

with the samplings satisfying the relation

$$\Delta t\, \Delta\omega = \frac{2\pi}{N}. \tag{6}$$

Since $T = N\Delta t$ and $\Delta\omega = 2\pi/T$, from the above relation, the frequency resolution is given by

$$\Delta f = \frac{\Delta\omega}{2\pi} = \frac{1}{T}. \tag{7}$$

Now the integral is replaced by a discrete sum. The discretization in frequency introduces periodicity of T in time with the result being a time-shifted sum of all the periodic responses [3],

$$\begin{aligned} &\sum_n p(r, z, t_i + nT) \\ &\quad = \Delta\omega \sum_{l=-(N/2-1)}^{N/2-1} S(\omega_l)[P(r, z, \omega_l) e^{i t_{min}\omega_l}] e^{i\frac{2\pi li}{N}} \end{aligned} \tag{8}$$

or by using the conjugate-symmetric property of the transfer function,

$$\begin{aligned} &\sum_n p(r, z, t_i + nT) \\ &\quad = \Delta\omega\, \mathrm{Re}\{\sum_{l=0}^{N/2-1} \varepsilon_l S(\omega_l)[P(r, z, \omega_l) e^{i t_{min}\omega_l}] e^{i\frac{2\pi li}{N}}\} \end{aligned} \tag{9}$$

with $\varepsilon_l = 1$ (for $l = 0$) or 2 (for $l > 0$).

The actual response in the selected time window $[t_{min}, t_{min} + T]$ then becomes

$$\begin{aligned} p(r, z, t_i) &= \Delta\omega\, \mathrm{Re}\{\sum_{l=0}^{N/2-1} \varepsilon_l S(\omega)[P(r, z, \omega_l) e^{i t_{min}\omega_l}] e^{i\frac{2\pi li}{N}} \\ &\quad - \sum_{n\neq 0} p(r, z, t_i + nT), \end{aligned} \tag{10}$$

where the last term denotes the wrap-around or aliasing from the periodic time windows. Main effort to obtain time signals in Eq.(10) is devoted to computing pressure field $P(r, z, \omega)$ in each spatial grid and frequency. This is performed with an acoustic model based on the PE scheme. In the simulation the center frequency is chosen

as 200 Hz and the sampling frequency as 1024 Hz which satisfies the Nyquist criterion.

B. Pseudo Wigner-Ville Distribution (PWVD)

We need a spectrum estimator to analyze the time signal obtained by Eq. (10). The PWVD is mathematically sophisticated approach capable of higher resolution for a given length of data. This is a kind of time-frequency distributions and is known to be suitable for analyzing transient or other non-stationary phenomena. It has been widely used in optics [4-6] and speech processing [7, 8] mainly because it promises high resolution in frequency and time.

The Wigner-Ville distribution (WVD) of signal $s(t)$ is defined as [9]

$$W(t,\omega)=\int_{-\infty}^{\infty} s^*\left(t-\frac{\tau}{2}\right)s\left(t+\frac{\tau}{2}\right)e^{j\omega\tau}d\tau, \tag{11}$$

and discrete time form as [10]

$$W(t,\omega)=2\sum_{\tau=-\infty}^{\infty} s^*\left(t-\frac{\tau}{2}\right)s\left(t+\frac{\tau}{2}\right)e^{-j2\omega\tau}, \tag{12}$$

where $s^*(t)$ is the complex conjugate of signal $s(t)$.

For a sampled signal $s[n]\,(n=0,1,2,\ldots,N-1)$, Eq. (12) changes into

$$W[l,k]=\frac{1}{N}\sum_{n=0}^{N-1} s[l+n]\,s^*[l-n]\,e^{-j4\pi nk/N},\quad k=0,1,2,\ldots,N-1 \tag{13}$$

where $s[m]=0$ for $m<0$ and $m>N-1$.

Basically, Eq. (13) has the form of the FFT and one can utilize a FFT algorithm. However, Eq. (13) is rewritten to know what periodicity the WVD has.

$$\begin{aligned} W[l,k+m(N/2)] &= \frac{1}{N}\sum_{n=0}^{N-1} s[l+n]\,s^*[l-n]\,e^{-j\frac{4\pi n}{N}(k+m\frac{N}{2})} \\ &= \frac{1}{N}\sum_{n=0}^{N-1} s[l+n]\,s^*[l-n]\,e^{-j\frac{4\pi nk}{N}}e^{-j2\pi mn} \\ &= W[l,k] \end{aligned} \tag{14}$$

since $e^{-j2\pi mn}=1$ where m and n are integer.

From this relation it can be seen that the WVD has a periodicity of $N/2$. Hence, even when the sampled data $s[m]$ satisfies the Nyquist criterion there would be still aliasing component in the WVD. A simple way to avoid the aliasing is to introduce the analytic signal beforehand [11].

The analytic signal may be expressed by

$$s(t)=s_r(t)+jH\{s_r(t)\}, \tag{15}$$

where $H\{s_r(t)\}$ is the Hilbert transform and obtained convolving the impulse response $h(t)$ of $\pi/2$ phase shift as follows

$$H\{s_r(t)\}=s_r(t)*h(t), \tag{16}$$

where $h(t)=2\sin^2(\pi t/2)/\pi t, \quad t\neq 0$
$=0, \quad t=0.$

Since the WVD has a periodicity of $N/2$, Eq. (13) can be rewritten as follows

$$W[m\Delta t,k\Delta\omega]=2\Delta t\sum_{n=0}^{2N-1} s[(m+n)\Delta t]\,s^*[(m-n)\Delta t]\,e^{-j2\pi nk/2N}, \tag{17}$$

where $\Delta\omega=\pi/(2N\Delta t)$ and Δt is the sampling interval. In Eq. (17) the frequency resolution $\Delta\omega$ is 1/4 of the ordinary FFT, implying that the WDF guarantees four times of frequency resolution.

To suppress the interference arising from cross terms, a sliding window is applied in time-frequency domain. The WVD with a window is usually called the PWVD or smoothed WVD. The PWVD is obtained convolving the WDF with Gaussian window function G as follows

$$W'[l,m]=\frac{\Delta t\Delta\omega}{2\pi}\sum_{p=-l}^{N-l}\sum_{q=-k}^{N-k} W[p,q]\,G[p-l,q-m], \tag{18}$$

where $W'[l,m]$ is the PWVD, and

$$G[p,q]=\frac{1}{2\pi ik\Delta t\Delta\omega}\exp\left[-\left(\frac{p^2}{2i^2}+\frac{q^2}{2k^2}\right)\right]. \tag{19}$$

The signal $s[n]$ may be simulated pressure field or measured signal through sea experiment.

III. Simulated Signals

A. Input Data

To get distorted time signals, pressure fields satisfying the wave equation should be computed first by using a numerical model. The model is based on the PE scheme. It requires mainly three kinds of environmental input data: sound speed, density and attenuation. The time signals are obtained convolving source spectra with pressure fields as described in the theory.

The environment, on which time signal simulation is conducted, is a simple waveguide with pressure release surface and penetrable fluid bottom (Fig. 1). The source

depth is 30 m and source-receiver range is one of 5, 10, and 20 km. Two kinds of sound speed profile (SSP) are assumed and they are typical in winter and summer in shallow water. In the figure (Fig. 1b) it can be seen that the winter profile has actually one value of 1482 m/sec over the water depth. That is, the water was mixed well over the column. In winter, the surface water becomes denser because it loses heat by the wind from northwest that accelerates vertical mixing. The denser the surface water becomes, the easier it descends down the water column. On the other hand, the summer profile has negative gradient over the water depth, which being particularly large between 20 and 30 m. In summer the surface water is usually heated by the sun and thus it decreases in density. Consequently, the water column becomes more stable, meaning that it becomes more difficult to be mixed with the bottom water.

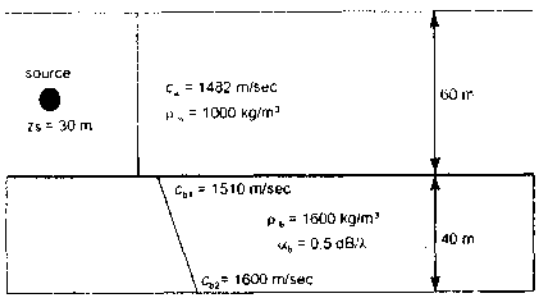

(a) geoacoustic data

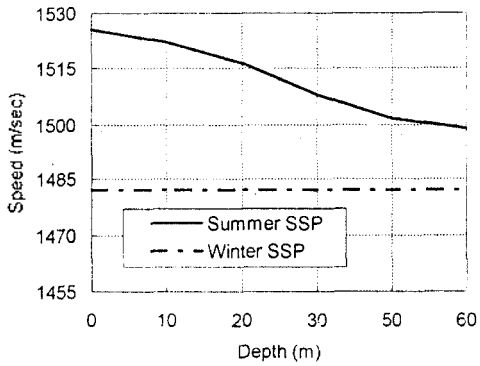

(b) sound speed profile

Figural 1. Input data used for the time signal simulations.

The sediment parameters are shown in the figure including sound speed (c_b), density (ρ_b), and attenuation (α_b). They are determined by referring to Miller and Wolf [12]. The bottom properties are crucial to sound wave propagation in shallow water because of the frequent interactions of the waves with the bottom. The acoustic model requires sound speed, attenuation coefficient, density, and possibly shear speed. Most of these parameters, however, are not available at the desired site because marine geology is rather complex and not well known. Shear wave propagation in the bottom layer is not included based on the studies [13, 14] showing that the effect of the low shear speed (below 300 m/sec) on sound wave propagation in the water layer is weak and negligible.

B. Generation of LFM Signals

Once the pressure fields are computed by the model they are convolved with source signals to give received signals at each depth and range. The source signal is assumed to be projected from the source while received ones to be distorted by the environment through which the acoustic waves travel.

This study considers a LFM signal of which center frequency is 200 Hz and bandwidth is 100 Hz so that the signal sweeps up or down in 150-250 Hz. The LFM signal, $s(t)$, is generated by the following equation [15]

$$s(t) = \sin[2\pi(f_o t + mt^2/2)], \tag{20}$$

where f_o = center frequency (200 Hz), m = bandwidth (100 Hz). For the upsweep signal the time goes from $-T/2$ to $T/2$ and for the downsweep signal from $T/2$ to $-T/2$. The sampling frequency is 1024 Hz so that 1024 sequences are generated over a period of one second.

Figure 2 gives waveforms of upsweep and downsweep signals over a period. Before the simulation of time signal a modified Hamming window is applied to the LFM signals generated by Eq. (20). This leads to reduce the energy leakage caused by the discontinuity of the finite record of data. The modified Hamming window is taken at the beginning and end of each 10% sweeping period as following:

$$w(t) = \begin{cases} 0.54 - 0.46\cos(10\pi t/T) & 0 \le t \le 0.1T, \\ 1.0 & 0.1T \le t \le 0.9T, \\ 0.54 - 0.46\cos[10\pi(T-t)/T] & 0.9T \le t \le T. \end{cases} \tag{21}$$

This kind of window is preferable since it modifies relatively small number of the signal compared with the ordinary window and so enables to keep LFM characteristics. Although the waveforms are different each other both classes of the signals have identical power spectra.

C. Results

Figure 3 presents some results of simulated signals at each range step. They are simulated with the winter SSP

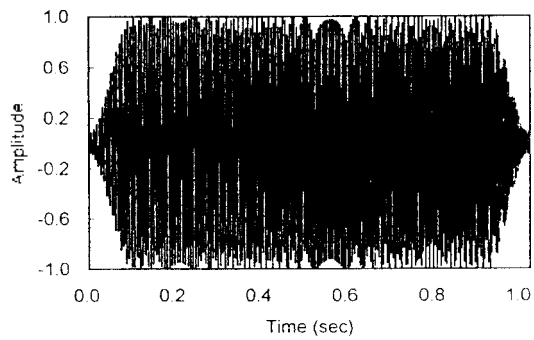

(a) upsweep

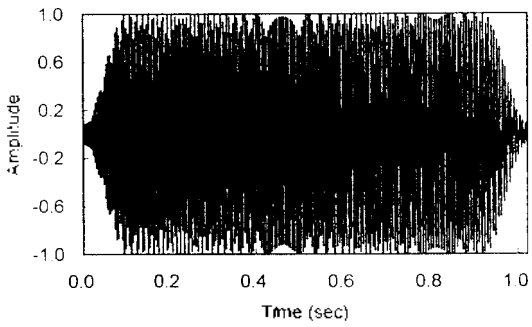

(b) downsweep

Figure 2. Waveform of the LFM signal swept up or down in 150-250Hz.

where the source signal is swept up. The figures give time-depth distributions of amplitude. The model inherently calculates the amplitudes over the whole layers of the water and sediment. In this study, however, the discussions are limited to the water layer because the amplitudes in the sediment layer are very small compared with those in the water layer. In the figures simulated amplitudes are magnified as much as 10^5 (or 100 dB).

In the amplitude distribution at range 5 km, it can be seen that there are noticeable constructive and destructive interference caused by the interactions among the propagating rays of neighboring frequency. The amplitudes are simulated with the upsweep signal. Some constructive interference spans up to more than 100 milliseconds. The interference may be accelerated by multi-paths of the rays with same frequency.

The result at range of 10 km (Fig. 3b) shows that there is still constructive interference and it is somewhat symmetric over the water depth. The amplitudes are simulated with the upsweep signal. The duration time of the interference tends to decrease compared with that at range 5 km. In the result at range of 20 km (Fig. 3c), the duration time of the interference decreases much more, while the symmetricity increases over depth. The amplitudes are also simulated with the upsweep signal.

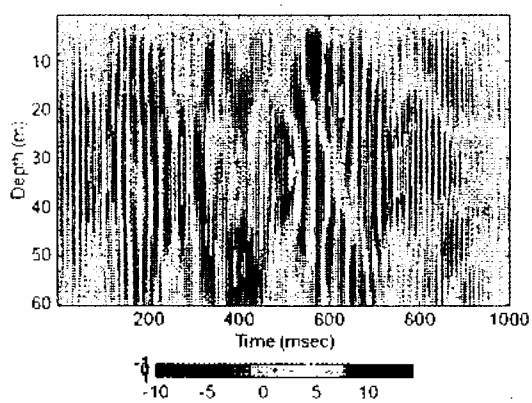

(a) range 5 km, upsweep

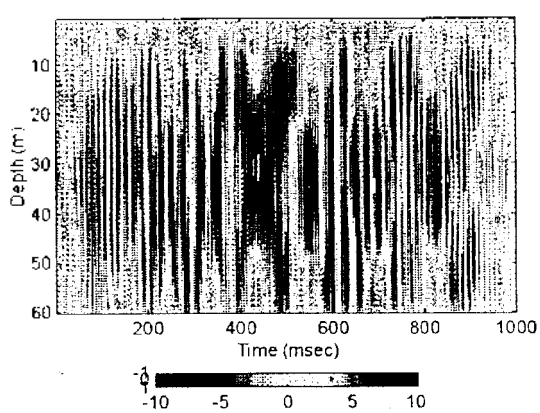

(b) range 10 km, upsweep

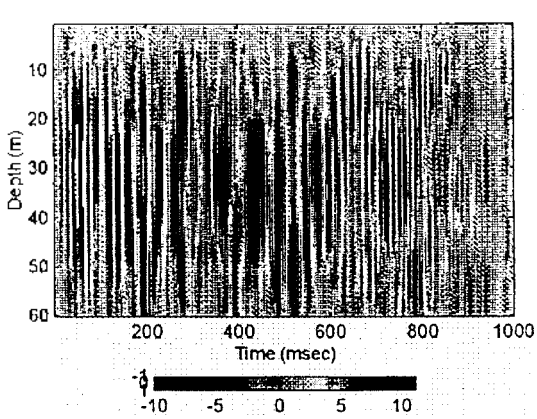

(c) range 20 km, upsweep

Figure 3. Simulated amplitude distributions with time and depth for the various ranges. Amplitudes are simulated with the winter SSP and are amplified by 10^5.

There exists noticeable destructive interference near the surface and the bottom and this is explainable by the reflection between the two interfaces. Large difference in impedance between air and water causes nearly perfect reflection with an angle-dependent phase shift. This mechanism makes the waves superpose themselves to result in destructive interference. For the other interference between water and bottom sediment the reflection coefficient can be estimated based on the geoacoustic parameters in Fig. 1. At low grazing angles of below 5° it can be shown that the reflection coefficient is almost 1.0 [16], implying perfect reflection toward water layer and then destructive interference between the incident and reflected waves.

In the PWVD examples at the receiver depth of 30 m (Fig. 4) one can see time varying patterns of LFM signal, but strong constructive and destructive interference. The three PWVDs come from the three amplitude distributions in Fig. 3. In the figure some constructive interference exists on almost one frequency with time, implying resonance resulted from interaction among the rays of neighboring frequencies. This phenomenon is the most profound in the result at range of 5 km.

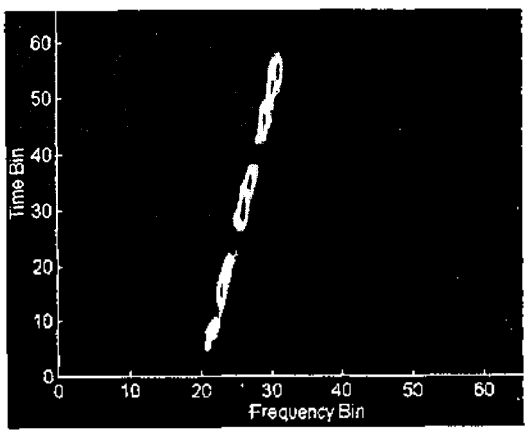

(a) range 5 km, upsweep

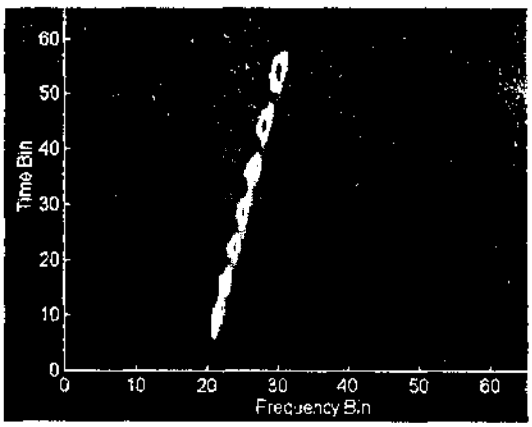

(b) range 10 km, upsweep

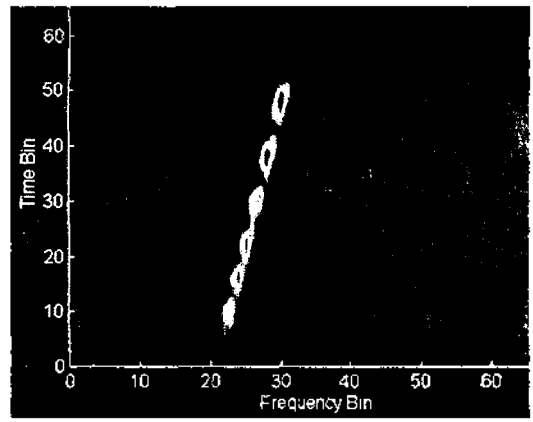

(c) range 20 km, upsweep

Figure 4. Spectrograms of the signal via the PWVD at the receiver depth of 30 m.

Meanwhile, the amplitudes simulated with the summer SSP (Fig. 5) show large difference compared with those with the winter profile. At a glance, most of constructive interference occurs at lower depth. As can be seen in Fig. 1 the summer SSP has strong negative gradient over depth (particularly in depth 20-30 m) and thus most of traveling waves are refracted into the lower part. As a result, the symmetricity over water depth, which is typical for the winter SSP, is destroyed at longer ranges.

IV. Measured Signals

A. Sea Experiment

In the sea experiment one sound source and three receivers were used. The sound source projected four LFM

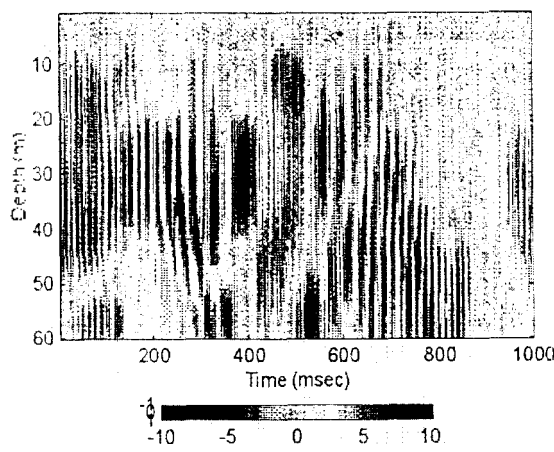

(a) range 5 km, upsweep

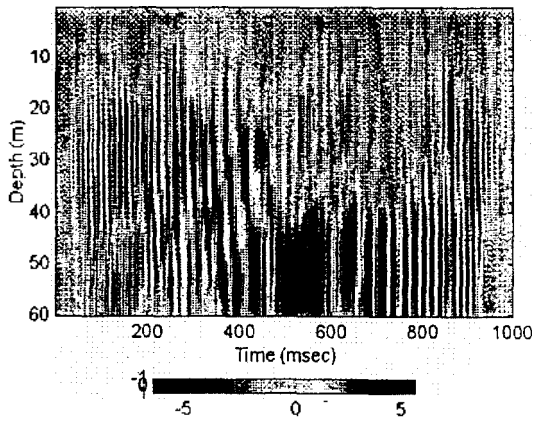

(b) range 10 km, downsweep

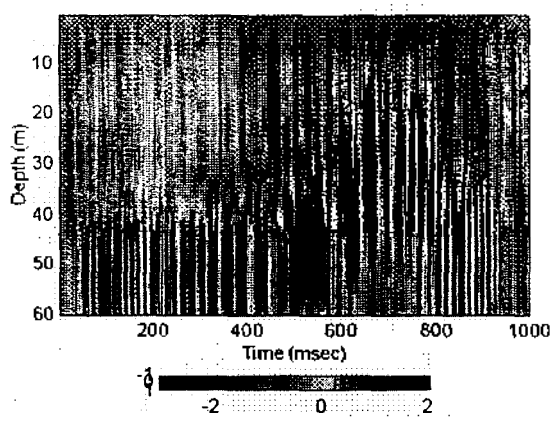

(c) range 20 km, downsweep

Figure 5. Simulated amplitude distributions with time and depth for the various ranges. Amplitudes are simulated with the summer SSP and are amplified by 10^5.

signals centered on 200, 400, 600 and 800 Hz with each bandwidth of 100 Hz. The signals were swept up for one second and down for an another second. That is, they were repeated to produce the two classes of LFM signals every two seconds. To check the quality of the projected signals, a hydrophone was installed at 1 m away from the source and made to monitor the signals. The source was operated on the water depths of 10 and 30 m. A CTD (conductivity, temperature and depth) equipment was also deployed to get oceanographic data for resolving water conditions. The experiment was conducted on March. A few days before the experiment there was wind from northwest and it was strong enough to mix the whole water column.

The sound source produced signals for more than 15 minutes at each depth. The source-receiver range was about 5.4 km. Two kinds of receivers, the sonobuoy AN/SSQ-57A (DRR1, 2) and sonobuoy AN/SSQ-57B (BMR), were used. The latter was modified so that it could separate received signals into the north-south and east-west components. Two sonobuoys (DRR1, 2) were connected each other by a 100 m-long rope and allowed to drift in water, keeping water depth of about 18 m. However, they were again connected to the weight on the sea bottom via the rope so that they could drift in a limited area. The modified receiver (BMR) was installed on the sea bottom where the depth is around 60 m. Figure 6 presents the schema of the source and receiver configuration. The received signals were transmitted to the land site via radio frequency where they were recorded for further processing. An acoustic release was used to make ease the recovery. It operates to release weight in the recovering stage responding to the coded acoustic signal from the surface.

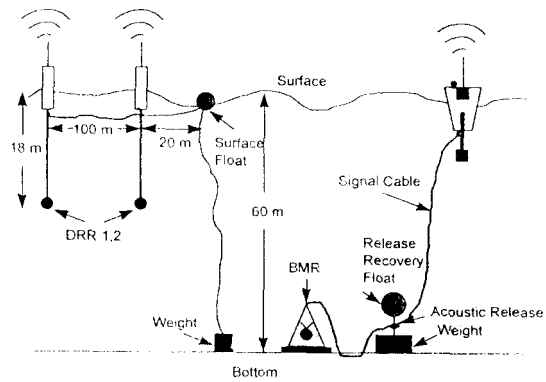

Figure 6. Installation of the receivers for the experiment.

B. Environmental Condition

The bottom of the experiment area consists of sand-silt-clay. Its typical geoacoustic parameters are characterized by density 1600 kg/m^3, porosity 67.2%, sound speed 1510 m/sec, and attenuation coefficient 0.5 dB/λ [12]. The winter SSP in Fig. 1 comes from the measured data through a CTD equipment. The profile shows typical pattern of very well mixed water, remaining almost the same speed from the surface to the bottom. This pattern was caused by the strong wind from northwest a few days before the experiment.

Ray traveling patterns may be simulated with the measured SSP. The source depth is assumed to be 30 m. As can be seen in Fig. 7 all rays interact with the surface and the bottom at least six times over the range 20 km.

C. Results

The received time signals are assumed to suffer distortion by the environment through which they travel. In addition, they are corrupted by some noise of which characteristics are hard to be defined. This section is de-

voted to analyzing measured signals and comparing them with the simulated ones.

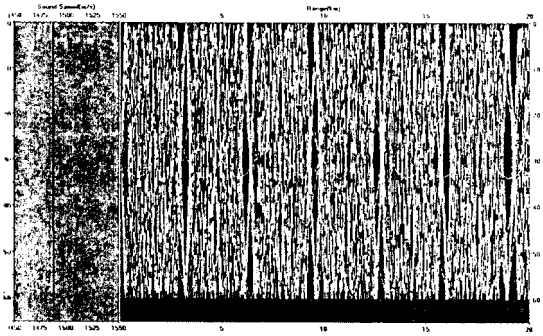

Figure 7. Ray tracing result with the measured SSP during the experiment. The source depth is 30 m

Figure 8 presents an example of the PWVD of the signals monitored at 1 m away from the source. In this case the signal was swept down. It was to check the quality of the projected signal with time. In the figure the frequency and time axes span 256 bins, representing 1024 Hz and one second, respectively. Each LFM signal has the bandwidth of 100 Hz. Among the four LFM signals the one with center frequency of 600 Hz is the most intensive (i.e., signal to noise ratio is the highest). Even in a 1-second period one can see that there is intensity variation with time, particularly in the fourth LFM signal of which center frequency is 800 Hz.

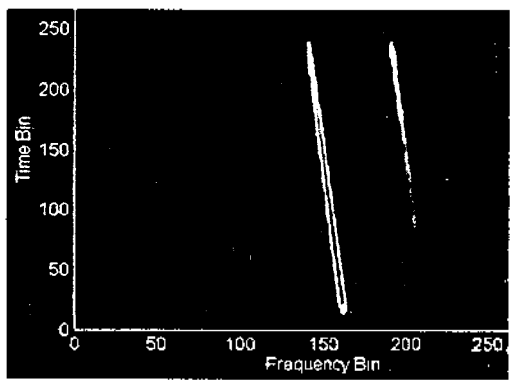

Figure 8. A PWVD of the downsweep signal monitored at 1 m away from the source. The center frequencies of the four LFM signals are 200, 400, 600, and 800 Hz with the bandwidth of 100 Hz.

An example of the received signal at 5.4 km away from the source (Fig. 9) shows that there are obvious four LFM signals. In this example the signal was swept down. As shown in the monitored signal the third LFM signal has the strongest intensity. The frequency and time axes correspond to 1024 Hz and one second, respectively. It is via the PWVD for the signals at the depth of 60 m.

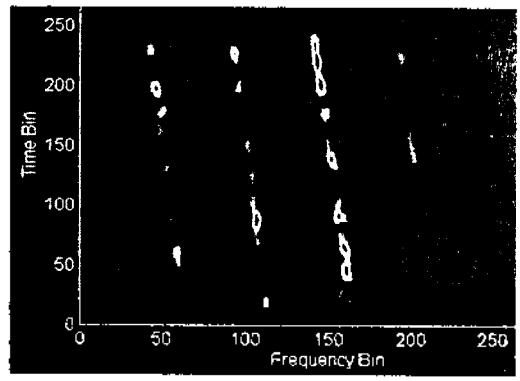

Figure 9. A PWVD of the received downsweep signal at the depth of 60 m and 5.4 km away from the source. The center frequencies of the four LFM signals are 200, 400, 600, and 800 Hz with the bandwidth of 100 Hz.

Figure 10 shows two waveforms and their PWVDs. The frequency axis denotes the range 0-512 Hz and the time axis one second. The waveforms are derived applying the band-pass filter to the received signals. A finite impulse response (FIR) filter [17] is introduced to extract each LFM signal from the received signals. The length of the FIR filter is specified by L = 20 and the band edges are 100 and 300 Hz. Consequently, only the signal of center frequency 200 Hz will remain after filtering. Although not so strong as in the simulated cases the waveforms show constructive or destructive interference which can be verified through their PWVDs. By examining the PWVDs one can see the resonance, which develops largely in magnitude but keeps almost the same frequency with time.

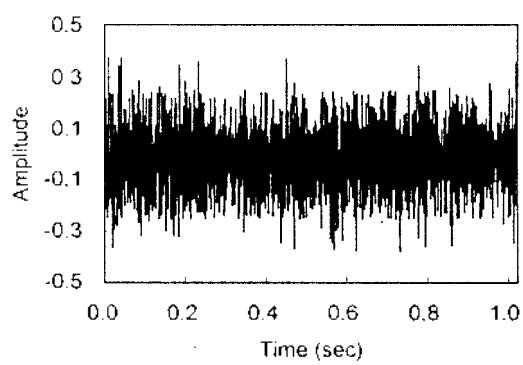

(a) waveform of upsweep signal

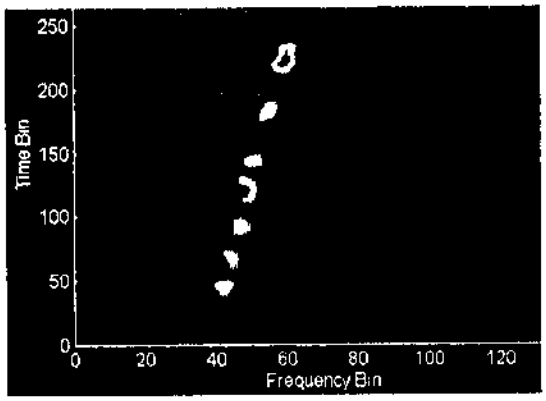

(b) PWVD of the upsweep signal

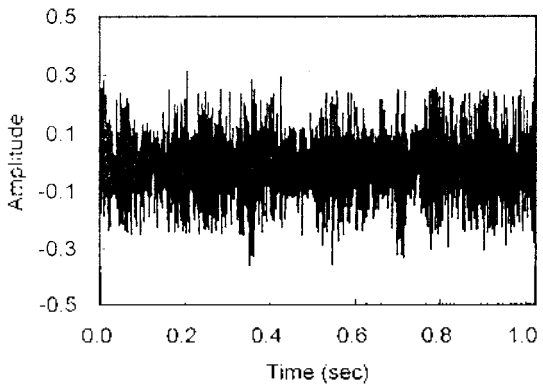

(c) waveform of downsweep signal

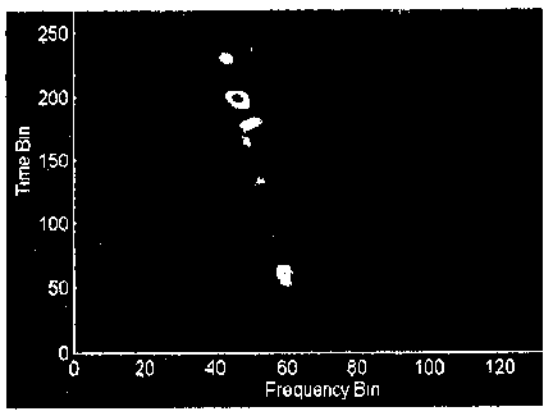

(d) PWVD of downsweep signal

Figure 10. Examples of waveform and spectrogram via the PWVD on the received signals. The signals are band-pass filtered on 100-300 Hz

By identifying eigenrays [18] one can see that there exist 6 main rays of relatively small loss and they make about 4 milliseconds difference in the arrival time over the distance of 5.4 km (Table 1). The 6 eigenrays make angles of less than 3° from the horizontal, and they undergo up to two interactions with the surface or bottom. The ray arriving first at the receiver undergoes only one surface reflection, so it is expected to have minimum propagation loss. However, the model shows that the ray, interacting once with the surface and bottom, may have minimum loss of −77.29 dB. The loss mechanisms include traveling path length and attenuation in addition to reflections. Moreover, the bottom loss by reflection itself varies with the incidence angle.

Table 1. Six eigenrays of relatively small propagation loss over the horizontal range of 5.4 km

Time (sec)	Source Angle(deg)	Receiver Angle(deg)	Level (dB)	*NSRF	'NBRF
3.644	0.950	0.934	78.56	1	0
3.645	1.590	1.581	−77.29	1	1
3.645	1.594	−1.585	79.99	1	2
3.646	2.229	2.222	−77.59	2	1
3.646	2.223	−2.226	−79.54	2	2
3.648	2.865	2.860	79.41	2	2

(*) No. of surface reflection
(') No. of bottom reflection

Like the simulated one the real signal keeps LFM characteristics well over the range. This can be explained by considering the fact that, in a shallow water, traveling rays inevitably interact with the surface and/or bottom, and a few of them contribute to the amplitude of received signal. Moreover, this study employs the LFM signals so that they have zero amplitudes at the beginning and end of a period. This effect reduces the problems of signal dispersion or elongation during long-range propagation. Generally, in shallow water, the rays arriving late may be thought to undergo more interactions with the two interfaces and consequently result in more propagation loss.

By referring to the model input parameters in Fig. 1 the low frequency cut-off can be estimated. The approximate modal solution for the Pakeris waveguide may be truncated to a few modes with real propagation wavenumbers. The mode number M increases with increasing frequency. When the frequency is lowered, the propagation wavenumber of a particular mode decreases. Assuming the Pakeris waveguide the low-frequency cut-off is determined by the relation [1]

$$f_{cm} = \frac{(m-0.5)\, c_w}{2D\sqrt{1-(c_w/c_b)^2}}, \qquad (22)$$

where D is water depth, m is mode number, c_w and

c_b are sound speeds in water and sediment, respectively. Using the parameters in Fig. 1 it can be shown that the first mode occurs at 16.4 Hz and the last at 245.7 Hz, total of 8 modes being excited below 250 Hz. The destructive or constructive interference may be also explained by the interactions of these modes.

V. Conclusions

Time signals are simulated using an acoustic model that employs the Fourier synthesis scheme. To obtain real sea data, an acoustic experiment has been performed in a shallow sea near Pohang, Korea.

The simulated time signals suffer great interference at range of 5 km by the interactions of neighboring rays. The simulated signals show great difference in amplitude distributions by the variation of SSP. Although there is constructive or destructive interference the received signals keep LFM characteristics. This property is thought to be caused by a few rays of small loss which contribute to the received signals in a shallow water environment.

Acknowledgements

The authors would like to appreciate Prof. J. Y. Na in Hanyang University for his useful comments. They wish to give thanks to Dr. J. J. Jeon in Agency for Defense Development for releasing programs on spectral estimation. Special thanks are directed to Dr. M. Collins in Naval Research Laboratory, USA for releasing a model that made it possible to simulate time signals. Their appreciation is extended to anonymous reviewers for their kind suggestions and comments.

References

1. F. B. Jensen, W. A. Kuperman, M. B. Porter, and H. Schmidt, "Broadband Modeling," in Computational Ocean Acoustics, AIP Press, Woodbury, NY, 1994.
2. R. L. Field, E. J. Yoerger, and P. K. Simpson, "Performance of Neural Networks in Classifying Environmentally Distorted Transient Signals," Oceans'90 Proc., pp.13-17, 1991.
3. A. V. Oppenheim and R. W. Schafer, Discrete-Time Signal Processing, Prentice Hall, New Jersey, 1989.
4. M. J. Bastians, "The Wigner Distribution Function Applied to Optic Signals and Systems," *Optics Comm.*, vol.25(1), pp.26-30, 1978.
5. M. J. Bastians, "Wigner Distribution Function and Its Application to First-Order Optics," *J. Optic. Soc. Am.*, vol.69 (12), pp.1710-1716, 1979.
6. H. O. Bartlet, K. H. Brenner, and A. W. Lohmann, "The Wigner Distribution Function and Its Optical Production," *Optics Comm.*, vol.32(11), pp.32-38, 1980.
7. M. Riley, Speech Time-Frequency Representations, Kluwer Academic Publishers, 1989.
8. E. Velez and R. Absher, "Transient Analysis of Speech Signals Using the Wigner Time-Frequency Representation," *IEEE Intl. Conf. Acoustics, Speech and Signal Processing*, vol.4, pp.2242-2245, 1989.
9. E. Wigner, "On the Quantum Correction for Thermodynamic Equilibrium," *Physic Review*, vol.40, pp.740-759, 1932.
10. T. Classen and W. Mecklenbrauker, "The Wigner Distribution-A Tool for Time-Frequency Signal Analysis," *Philips J. Res.*, vol.35, part I : 217-250, part II : 276-300, part III : 372-389, 1980.
11. J. Ville, "Theorie et Applications de la Notion de Signal Analytique," *Cables et Transmission*, vol 29(1), pp.61-74, 1948.
12. J. F. Miller and S. N. Wolf, "Modal Acoustic Transmission Loss (MOATL) : A Transmission-Loss Computer Program Using a Normal-Mode Model of the Acoustic Field in the Ocean," Naval Research Lab., Rep. No. 8429, pp.1-126, 1980.
13. F. D. Tappert and T. Y. Yamamoto, "An issue (sediment volume fluctuations) and a non-issue (shear wave propagation) in shallow water acoustics," *J. Acoust. Soc. Am.*, vol. 93, p.2268A, 1993.
14. C. T. Tindle and Z. Y. Zhang, "An equivalent fluid approximation for a low shear speed ocean bottom," *J. Acoust. Soc. Am.*, vol.91, pp.3248-3256, 1992.
15. R. O. Nielson, Sonar Signal Processing, Artech House Inc., Boston, 1991.
16. Y. N. Na, Classification of Environmentally Distorted Acoustic Signals in Shallow Water Using Neural Networks, Ph. D. Thesis in Pukyong National University, Pusan, pp. 1-202, 1998.
17. S. D. Stearns and R. A. David, Signal Processing Algorithms in Fortran and C, Prentice Hall International Inc., pp.1-331, 1993.
18. S.W. Shin, Study on Ray-Method Model based on Constant-Gradient Sound Speed, Master Thesis in Hanyang University, pp. 1-54, 1994.

▲Young-Nam Na
Senior Research Scientist, Agency for Defense Development (Vol. 15, No. 3E, 1996)

▲Mun-Sub Jurng
Senior Research Scientist, Agency for Defense Development (Vol. 13, No. 2E, 1994)

▲Taebo Shim
Chief Research Scientist, Agency for Defense Development (Vol. 14, No. 2E, 1995)

▲Chun-Duck Kim
Professor, Department of Electrical Engineering Pukyong National University (Vol. 15, No. 3E, 1996)